



## OPEN Research on reasonable length of steeply dipping coal seam working face based on the fuzzy comprehensive evaluation method

Huiyang Zhang<sup>1</sup>, Zhongping Guo<sup>1</sup>✉, Fei Ma<sup>2</sup> & Yuanchao Liu<sup>3</sup>

The study employed the Analytic Hierarchy Process, Coefficient of Variation method, and fuzzy mathematics to determine the optimal working face length through evaluation of six key cost factors. The application of economic optimization principles and operational safety standards yielded an optimal working face length of 260 m. Numerical simulations and field data indicate that the 260 m working face achieves lower roof stress levels and reduced machinery wear. Field tests demonstrated that the roof subsidence was maintained below 0.37 m, with higher consistency between the predicted and actual stress distributions, validating the reliability of the method for the working face length in steeply dipping coal seams.

**Keywords** Coal, Working face length, Analytic hierarchy process, Fuzzy evaluation method, Economic costs

Mining steeply dipping coal seams (dip angles 35°–55°) presents challenges including increased mining-induced stress, rock instability<sup>1</sup>, and risks of rib spalling and roof collapse<sup>2</sup>. These conditions affect both safety and productivity. Appropriate mining parameters can help mitigate these risks, with working face length optimization being a key factor in steeply dipping<sup>3</sup>, fully mechanized mining operations<sup>4</sup>. The determination of optimal working face length is therefore important in mine design and planning<sup>5</sup>.

Existing research has advanced our understanding of how working face length affects mining operations through various methodological approaches. Wang et al.<sup>6</sup> determined that optimal roof control in thick coal seams occurs within the 140–155 m range using integrated numerical simulations and field measurements. Ordín et al.<sup>7</sup> established that geological conditions play a decisive role in determining economically viable face lengths. Zhao G. et al.<sup>8</sup> found face elongation has limited effects on roof fracture characteristics, while Xue B. et al.<sup>9</sup> showed support parameters are critical for coal wall stability under large mining heights. Zhang J. et al.<sup>10</sup> showed that longer face lengths reduce roof stability due to increased deflection, and Ding Z. et al.<sup>11</sup> quantified overburden movement at 300 m face lengths. Wang H. et al.<sup>12</sup> observed that longer faces change support stress from single-peak to multi-peak patterns, especially at 300 m. Meng G. H. et al.<sup>13</sup> found that face elongation alters support resistance distribution in ultra-long faces. Huang P. et al.<sup>14</sup> linked longer faces to larger pillar sizes, improving resource recovery, while Wang X. et al.<sup>15</sup> described crack development under different face lengths. Other studies examined related aspects: Tong X. et al.<sup>16</sup> and Liu X. et al.<sup>17</sup> studied geological detection and subsidence control. Liu B. et al.<sup>18</sup> reported reduced oxygen levels in ultra-long faces due to longer airflow paths. In summary, it can be seen that previous research on working face length has typically examined individual technical factors such as roof fractures or support resistance, primarily in shallow coal seams<sup>19</sup>. These studies seldom integrate safety and economic considerations, including equipment, relocation, and maintenance costs. This limitation is particularly evident in steeply dipping seams, where complex geological conditions require holistic approaches<sup>20</sup>.

Based on existing research, This study focuses on the key cost parameters of the working face and develops a methodology using fuzzy AHP weighting, numerical simulation, and field measurements. An evaluation framework is established that incorporates both safety and costs factors to determine the optimal working face length in steeply dipping coal seams<sup>21</sup>. This approach provides a balanced strategy for safe and economically viable mining under geologically challenging conditions.

<sup>1</sup>School of Energy and Mining Engineering, Shandong University of Science and Technology, Qingdao 266590, Shandong, China. <sup>2</sup>Zhaizhen Coal Mine, Xinwen Mining Group Co., Ltd., Xintai 271200, Shandong, China. <sup>3</sup>Erdos, Ettok Qianqi Great Wall No. 3 Mining Co., Ltd., Inner Mongolia 017000, China. ✉email: 17866831691@163.com

## Factors affecting working face length

Optimal working face length determination is critical for scientifically establishing initial mining parameters and ensuring mine output. A moderate length increase enhances recoverable coal resources and production capacity. However, excessive length reduces the advancement speed, intensifies mine pressure manifestations, and increases the occurrence of roof collapse incidents. Achieving production target requires systematic face length analysis to ensure high efficiency and productivity of the mining operation. Steeply dipping coal seams can cause the equipment to slide and move out of position during mining. An insufficient face length triggers frequent equipment adjustments, elevates end-area stress concentration and increases roof collapse risks. The working face length should ensure continuous and reliable equipment operation, typically requiring at least 150 m. Field data indicates that the minimum length of a steeply dipping comprehensive mining working face is generally set at approximately 150–180 m to ensure the efficient equipment operation. Thicker seams typically require 150–200 m minimum length. When productivity is higher, the costs per ton of coal are lower, and safety and reliability are higher. Analysis concludes steeply dipping slopes can set minimum face length at 180 m.

## Relationship between the working face length and cost parameters

Working face length variations directly influence cost parameters, causing corresponding fluctuations in overall expenses. The six cost indicators used in this study (relocation, equipment, labor, tunneling, maintenance, and transportation costs) are based on life-cycle cost theory, covering the complete investment, production, and replacement cycle. The selection of these costs aligns with coal mining characteristics. Relocation costs reflect the cyclical nature of face retreat and advancement. Equipment and tunneling represent major capital investments. Labor and maintenance are essential for sustained and safe operations, while transportation efficiency determines logistical performance. This framework combines theoretical rigor with industry-specific relevance.

Relocation costs cover equipment transfer between working faces. Short faces require frequent moves, increasing costs. When the working face is long, although relocation frequency decreases, costs increase with increased workload per move.

Equipment costs rise by 15–20% per 100 m extension for additional equipment. Shorter faces reduce equipment utilization and increase unit production costs.

Labor costs include wages for the operators and maintenance staff. Longer face spans require more workers, increasing overall labor costs; shorter face spans reduce worker efficiency and increase unit labor costs.

Tunneling costs decrease with longer faces due to reduced total roadway length, improved equipment utilization, and fewer moves. Shorter lengths reduce roadway utilization and increase the unit cost of tunneling.

Transport expenses for coal haulage rise with longer faces due to increased distance. Short haulage distances lead to under utilization of haulage systems and equipment and increase unit costs.

Maintenance costs cover equipment and roadway upkeep. Longer faces increase maintenance workload and costs. Shorter face spans may increase maintenance frequency due to frequent equipment adjustments, increasing unit costs.

## Study on the appropriate working face length

Based on current mining face conditions, the cost parameters influencing working face length were evaluated. The fuzzy comprehensive evaluation model used the factor set  $U$  containing six cost indicators: relocation, equipment, labor, tunneling, maintenance, and transportation. This study selected working face lengths of 200 m, 240 m, 280 m, 320 m and 360 m as evaluation points. These values represent mainstream mining configurations and correspond to critical technical thresholds. The 200 m length meets basic safety requirements, while 240 m aligns with optimal equipment economics. Lengths exceeding 280 m exhibit nonlinear increases in rock pressure and maintenance costs. This selection enables the model to capture qualitative changes across different length regimes.

The Analytic Hierarchy Process (AHP), developed by Thomas L. Saaty, structures multi-criteria decisions through pairwise comparisons. Using Saaty's 1–9 ratio scale, qualitative judgments are quantified to form a judgment matrix for evaluating cost parameters hierarchically<sup>22</sup>. Scales 1–9 are presented in Table 1.

Fifteen mining experts evaluated the parameters to ensure objectivity, with results cross-validated against historical data from five mines. The comparative analysis of cost parameters' relative importance formed a  $6 \times 6$  judgment matrix  $A$ .

Scale $a_{ij}$	Scale $a_{ij}$
1	Element $i$ is just as important as element $j$
3	Element $i$ is slightly more important than element $j$
5	Element $i$ is obviously more important than element $j$
7	Element $i$ is more important than element $j$
9	Element $i$ is more important than element $j$
2, 4, 6, 8	Is the intermediate value of the above adjacent judgment
Reciprocal ( $1/a_{ij}$ )	$1/a_{ij}$ indicates the result of comparing element $j$ with element $i$

**Table 1.** 1-9 Scaling method.

$$A = \begin{bmatrix} 1 & \frac{1}{5} & \frac{1}{5} & \frac{1}{3} & \frac{1}{2} & \frac{1}{3} \\ 5 & 1 & 2 & 2 & 2 & 2 \\ 3 & \frac{1}{2} & 1 & 1 & 2 & 2 \\ 2 & \frac{1}{3} & \frac{1}{2} & 1 & 1 & 1 \\ 2 & \frac{1}{3} & \frac{1}{2} & 1 & 1 & 1 \end{bmatrix}$$

**Calculate weight using the arithmetic average method**

The judgment matrix elements were normalized using Saaty’s eigenvector method, with row sums calculated from the normalized results<sup>23</sup>.

$$W_1 = \frac{1}{n} \sum_{j=1}^n \frac{a_{ij}}{\sum_{k=1}^n a_{kj}} \quad (i = 1, 2, \dots, n) \tag{1}$$

where dim(a) is the matrix order;

Calculated:  $W_1 = [ 0.073 \quad 0.104 \quad 0.313 \quad 0.218 \quad 0.152 \quad 0.140 ]^T$

Expert judgments may produce inconsistent matrices due to problem complexity and perceptual ambiguity, requiring a consistency check. A consistency ratio (CR) < 0.1 indicates acceptable consistency; if CR ≥ 0.1, weights undergo iterative recalculation with score adjustment until CR < 0.1. Table 2 provides the random consistency indices (RI) for different matrix orders.

The maximum eigenvalue  $\lambda_{max}$  and index *CI* of the evaluation matrix A is calculated as follows: The consistency ratio *CR* of judgment matrix A is calculated according to the Eq. <sup>24</sup>.

$$\lambda_{max} = \sum \frac{(A \times W)_i}{nW_i} \tag{2}$$

$$CI = \frac{\lambda_{max} - n}{n - 1} \tag{3}$$

Calculated  $\lambda_{max} = 6.132$ .

*CI* = 0.0264.

From Table 2 obtain the random index RI = 1.24 for n = 6.

$$CR = \frac{CI}{RI} \tag{4}$$

Judgment matrix A has acceptable consistency only when CR < 0.1; if CR ≥ 0.1, it indicates that judgment matrix A should be adjusted accordingly.

Calculated CR = 0.0213 < 0.1

**Coefficient of variation method**

The coefficient of variation (CV) method weights indicators by quantifying data variability. Weights reflect the deviation between current and target values—larger deviations receive higher weights as they indicate greater difficulty in achieving targets. Normalized deviations below 0.1 receive reduced weights. The data from working faces under varying geological conditions were collected and normalized to a [0,1] range using min–max scaling. Table 3 presents the standardized costs data from eight mining cases.

*Calculate mean and standard deviation*

The mean of indicator j is calculated by summing its values across all samples and dividing by the sample size n. The standard deviation is then derived by computing the square root of the average squared difference between each value and the mean, using n-1 as the denominator. These metrics respectively reflect the central tendency and dispersion of indicator j<sup>25</sup>.

$$\bar{x}_j = \frac{1}{n} \sum_{i=1}^n x_{ij} \tag{5}$$

$$S_j = \sqrt{\frac{\sum_{i=1}^n (x_{ij} - \bar{x}_j)^2}{n - 1}} \tag{6}$$

Matrix order Number n	1	2	3	4	5	6	7	8	9	10
RI	0.00	0.00	0.58	0.90	1.12	1.24	1.32	1.41	1.45	1.49

**Table 2.** Consistency indicators.

Parameter	Labor costs	Transportation costs	Maintenance costs	Tunneling costs	Equipment costs	Relocation costs
A <sub>1</sub>	0.078	0.108	0.215	0.242	0.207	0.150
A <sub>2</sub>	0.080	0.100	0.170	0.260	0.200	0.190
B <sub>1</sub>	0.085	0.115	0.230	0.235	0.215	0.120
B <sub>2</sub>	0.084	0.113	0.221	0.229	0.211	0.142
C <sub>1</sub>	0.090	0.130	0.240	0.210	0.230	0.100
C <sub>2</sub>	0.082	0.122	0.225	0.231	0.208	0.132
D <sub>1</sub>	0.076	0.104	0.209	0.238	0.204	0.169
D <sub>2</sub>	0.072	0.100	0.200	0.228	0.200	0.200
E <sub>1</sub>	0.082	0.117	0.219	0.227	0.216	0.139
E <sub>2</sub>	0.078	0.106	0.216	0.234	0.206	0.160

**Table 3.** Sample data.

Project	Average value	Standard deviation	Coefficient of variation	Weight
Labor costs	0.080	0.010	0.125	0.185
Transportation costs	0.110	0.010	0.091	0.135
Maintenance costs	0.220	0.026	0.120	0.178
Tunneling costs	0.233	0.031	0.131	0.194
Equipment costs	0.203	0.015	0.075	0.111
Relocation costs	0.150	0.020	0.133	0.197

**Table 4.** Calculation results of coefficient of variation method.

*Calculate weights*

The CV for each indicator *j* is calculated as the ratio of its standard deviation *S<sub>j</sub>* to its mean. The weight of indicator *j* is then determined by dividing its CV value by the sum of the CV values for all *p* indicators, reflecting its relative importance within the indicator set.

$$v_j = \frac{S_j}{\bar{x}_j}, (j = 1, 2, \dots, p) \tag{7}$$

$$W_j = \frac{V_j}{\sum_{j=1}^p V_j} \tag{8}$$

Based on Eqs. (5), (6), (7), and (8) [26] the statistical results are shown in Table 4.

**Calculate the combination weight**

Subjective weighting methods rely on expert judgment but are prone to cognitive bias, while objective methods prioritize data analysis yet may overlook domain-specific contexts. To balance these limitations, combining AHP with CV method enhances weighting reliability and produces more robust results.

*Probability matrix creation*

The weight integration matrix *p* is constructed from the weight vectors obtained using the AHP and CV methods.

$$p_{ij} = \frac{w_{ij}}{\sum_{k=1}^n w_{kj}} \tag{9}$$

$$p = \begin{bmatrix} 0.073 & 0.185 \\ 0.104 & 0.135 \\ 0.313 & 0.178 \\ 0.218 & 0.194 \\ 0.152 & 0.111 \\ 0.140 & 0.197 \end{bmatrix}$$

Calculate the information entropy for each column vector

$$E_j = -k \sum_{i=1}^n p_{ij} \ln(p_{ij}), \quad k = \frac{1}{\ln(n)} \tag{10}$$

Calculated from equation:

$$k = 0.559; E_1 = 0.923; E_2 = 0.85.$$

Redundancy  $D_j$  represents the effective information of the weight method. It quantifies the information consistency of each method (range: 0–1)

$$d_j = 1 - E_j \quad (11)$$

Calculated from the equation.

$$d_1 = 0.077; d_2 = 0.15.$$

#### Combination coefficient

To ensure objectivity and minimize subjective bias, the coefficients were derived from a probability matrix using the entropy method<sup>27</sup>. The fundamental rationale behind this approach is that the entropy value can measure the amount of useful information provided by the data itself. A smaller entropy value for a specific indicator indicates a greater degree of variation in its data across different samples, which implies that this indicator transmits more information and plays a more significant role in the evaluation process. It should be assigned a higher weight. Normalize the above results to obtain the combination coefficient. Calculated from equation<sup>28</sup>:

$$\lambda_1 = \frac{d_1}{d_1 + d_2} \quad (12)$$

$$\lambda_2 = \frac{d_2}{d_1 + d_2} \quad (13)$$

$$\lambda_1 = 0.339; \lambda_2 = 0.661.$$

The combined weight  $W_3$  is calculated as:

$$W_3 = 0.339W_1 + 0.661W_2 = (0.147, 0.124, 0.22, 0.202, 0.125, 0.178).$$

### Working face cost parameters degree of affiliation analysis

Key costs are represented by membership degrees  $\mu(x) \in [0,1]$  within fuzzy sets. The membership function, a core concept in fuzzy logic, quantifies the degree to which an element belongs to a fuzzy set. It outputs a value between 0 (non-membership) and 1 (full membership), with intermediate values indicating partial membership. Common forms include triangular, trapezoidal, and Gaussian functions. To reasonably determine the membership function for working face cost parameters, the cost parameter function is selected as shown below based on cost characteristics.

(1) Based on coal mine data and existing research, labor costs increase linearly with working face length due to fixed staffing requirements. When the face length exceeds 280 m, production coordination becomes more difficult, reducing labor efficiency. The relationship is represented by the following segmented function<sup>29</sup>.

$$\mu_{people}(L) = \begin{cases} \frac{L-180}{100} & 180 \leq L \leq 280 \\ \frac{400-L}{120} & 280 < L \leq 400 \\ 0 & others \end{cases} \quad (14)$$

(2) Transportation costs rise with working face length. Below the transport system's design capacity, costs increase linearly. Achieving this capacity, accelerated equipment wear shifts the relationship to nonlinear. A segmented function models this relationship<sup>29</sup>.

$$\mu_{transportation}(L) = \begin{cases} \frac{L-180}{80} & 180 \leq L \leq 260 \\ e^{-0.02(L-260)} & 260 < L \leq 450 \\ 0 & others \end{cases} \quad (15)$$

(3) As a crucial component of the face operation costs, utilizing historical data from the mine and studies, When the face length exceeds 250 m, maintenance costs rise exponentially due to nonlinear growth in advance support pressure and deteriorating equipment conditions. This cost segmentation function is given by Eq. 16<sup>29</sup>.

$$\mu_{maintenance}(L) = \begin{cases} 1 - \frac{L-180}{70} & 180 \leq L \leq 250 \\ e^{-0.05(L-250)} & 250 < L \leq 450 \\ 0 & others \end{cases} \quad (16)$$

(4) Tunneling costs initially increase linearly with working face length. Beyond a critical length, engineering quantity decrease, causing costs to decline. Based on empirical analysis and existing research, the following segmented function is used to the relationship between face length and tunneling costs<sup>30</sup>.

$$\mu_{Tunneling}(L) = \begin{cases} 1 - \frac{L-180}{100} & 180 \leq L \leq 280 \\ 1 - e^{-0.01(L-280)} & 280 < L \leq 400 \\ 0 & others \end{cases} \quad (17)$$

(5) Equipment costs increase proportionally with working face length when equipment specifications remain unchanged. This relationship is represented using a segmented function<sup>30</sup>.

$$\mu_{equipment}(L) = \begin{cases} \frac{L-180}{70} & 180 \leq L \leq 250 \\ \frac{400-L}{110} & 250 < L \leq 360 \\ 0 & others \end{cases} \tag{18}$$

(6) Relocation costs increase linearly with working face length, determined by equipment quantity and relocation frequency. Based on the research data, the segmented function below is applied to illustrate the relationship between the working face length and relocation costs<sup>30</sup>.

$$\mu_{relocation}(L) = \begin{cases} \frac{L-180}{80} & 180 \leq L \leq 260 \\ \frac{400-L}{140} & 260 < L \leq 400 \\ 0 & others \end{cases} \tag{19}$$

Table 5 lists the membership degree of each cost parameters obtained according to the scheme corresponding to the membership function.

Establishing an evaluation matrix *f* from membership degree.

$$F = \begin{bmatrix} 0.2 & 0.25 & 0.75 & 0.8 & 0.286 & 0.25 \\ 0.6 & 0.75 & 0.143 & 0.4 & 0.857 & 0.75 \\ 1 & 0.67 & 0.223 & 0 & 0.727 & 0.857 \\ 0.667 & 0.301 & 0.03 & 0.330 & 0.364 & 0.571 \\ 0.333 & 0 & 0 & 0.551 & 0 & 0.286 \end{bmatrix}$$

The weight vector *W* obtained from the AHP undergoes matrix multiplication: *H* = *W* × *F*, to calculate the fuzzy evaluation score *H*, which is normalized to the 0 to 1 range. Score thresholds were calibrated via ROC analysis. Scores above 0.65 are classified as excellent, those between 0.4 and 0.65 as good and those below 0.4 as average.

$$B = F \times W_3$$

$$H_1 = 0.147 \cdot 0.2 + 0.124 \cdot 0.75 + 0.22 \cdot 0.8 + 0.202 \cdot 0.286 + 0.125 \cdot 0.25 + 0.178 \cdot 0.25 = 0.4319$$

$$H_2 = 0.147 \cdot 0.6 + 0.124 \cdot 0.75 + 0.22 \cdot 0.143 + 0.202 \cdot 0.4 + 0.125 \cdot 0.857 + 0.178 \cdot 0.75 = 0.5341.$$

$$H_3 = 0.147 \cdot 0.1 + 0.124 \cdot 0.67 + 0.22 \cdot 0.223 + 0.202 \cdot 0 + 0.125 \cdot 0.727 + 0.178 \cdot 0.857 = 0.3903.$$

$$H_4 = 0.147 \cdot 0.667 + 0.124 \cdot 0.301 + 0.22 \cdot 0.03 + 0.202 \cdot 0.33 + 0.125 \cdot 0.364 + 0.178 \cdot 0.571 = 0.3558.$$

$$H_5 = 0.147 \cdot 0.333 + 0.124 \cdot 0 + 0.22 \cdot 0 + 0.202 \cdot 0.551 + 0.125 \cdot 0 + 0.178 \cdot 0.286 = 0.2112.$$

Analysis of the comprehensive score shows a normal distribution pattern. The 260 m working face length achieves the highest overall score of 0.7072 within the 240–280 m range, making it the preferred design option. Statistical analysis of different mining face parameters reveals the relationship between unit production costs and face length in Fig. 1. The relationship between working face length and rock pressure is defined by elastic thin plate theory, which establishes that roof bending stress increases with the square of the length. This mechanical principle directly influences the costs evaluation model in this study. Figure 1 shows a sharp increase in total costs beyond the critical length of 260 m.

The polynomial fit of working face cost parameters showed high significance, confirming model reliability. Figure 1 indicates the economically optimal length for steeply dipping faces lies within 240–280 m, with costs increasing beyond 280 m. This costs inflection point results from rising rock pressure, which elevates multiple cost parameters: equipment maintenance increases due to accelerated wear, support costs grow with higher ground control requirements, and tunnel expenses rise with added roadway maintenance. The costs curve inflection point thus reflects the economic impact of mechanical principles. When the working face exceeds the critical length, the additional costs from higher rock pressure outweigh any economic benefits, setting the upper limit for the optimal length range. This study links rock pressure behavior to economic optimization in mining engineering. At this specific value, the marginal benefit of scale economies is exactly balanced by the marginal costs of diseconomies, resulting in the lowest costs per ton of coal and the highest return on investment. The mine’s production capacity, technical infrastructure, and economic efficiency collectively reach their practical operational limits at this value.

Scheme	Labor costs	Transportation costs	Maintenance costs	Tunneling costs	Equipment costs	Relocation costs
200	0.200	0.250	0.750	0.800	0.286	0.250
240	0.600	0.750	0.143	0.400	0.857	0.750
280	1	0.670	0.223	0	0.727	0.857
320	0.667	0.301	0.030	0.330	0.364	0.571
360	0.333	0	0	0.551	0	0.286

**Table 5.** Membership.

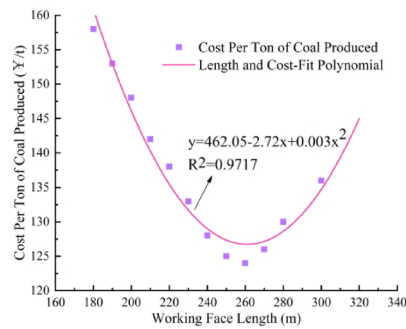


**Fig. 1.** Relationship between working face length and unit production costs.

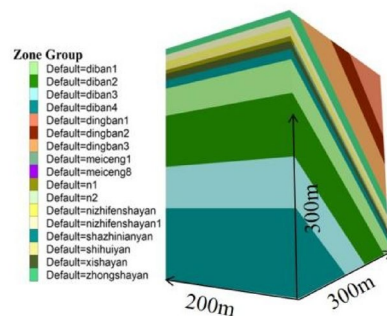


**Fig. 2.** Numerical simulation graph.

### Engineering analogy analysis

Near-horizontal coal seams exhibit small inclination angles with manageable roof conditions, enabling longer working faces that substantially improve mining efficiency and reduce unit costs. In contrast, steeply dipping seams ( $> 35^\circ$ ) pose distinct challenges as mining conditions become complicated, coal wall stability deteriorates significantly, and roof management becomes difficult, resulting in shorter working face lengths.

The Daliuta Coal Mine has an almost horizontal coal seam with less than  $3^\circ$  inclination. When the face length reaches 300 m, mining efficiency is greatly improved and economic benefits increase. The Yushwan Coal Mine has a near-level coal seam where working face length has been extended to enable large-scale mining, resulting in high-yield operations and significantly improved efficiency. In the Daizhuang coal mine, the maximum working face length exceeds 300 m. The economic efficiency of the mine improved significantly. Extended face length reduces the roadway development frequency and improves the equipment utilization.

The Lvshuiding coal mine has different conditions with an average coal seam inclination of  $45^\circ$  and maximum inclination of  $55^\circ$ , representing a typical large-inclination configuration. Engineering experience and historical data analysis support the conclusion that the optimal working face length is approximately 200 m. The Jinjiayu Coal Mine maintains a  $26^\circ$  average inclination, and after thorough evaluation of actual conditions, the optimized face length was set at 210 m. The Pangpangta Mine shows variable conditions; the working face length ranges from 200 to 250 m, and coal seam inclination varies between  $16^\circ$ – $38^\circ$ . Germany's Prosper-Haniel coal mine operates with a seam dip angle of  $30^\circ$  to  $40^\circ$ , where the longwall face reaches 270 m through new technologies and equipment. Australia's Peak Downs coal mine implemented special measures to test a 300 m face length in seams dipping  $25^\circ$  to  $35^\circ$ . Steeply dipping coal seams pose several challenges: flake ganging occurs on coal walls, roof management becomes complicated, and equipment operation becomes difficult on inclined faces. Therefore, owing to economic and safety constraints, the length of steeply dipping working faces is typically shorter than that of near-horizontal working faces.

### Numerical simulation analysis

A  $300 \times 200 \times 300$  m numerical model employed the Mohr–Coulomb constitutive model with a 260 m working face length. Boundary protection coal pillars were set at both strike ends and retained vertically to prevent boundary effects. The model applied a 12 MPa equivalent load to the top surface while fixing the sides and bottom with zero displacement/velocity constraints. The established numerical simulation structure appears in Fig. 2. The physical and mechanical parameters of coal seam roof and floor strata are selected from rock mechanics tests conducted in coal mines. The physical and mechanical parameters of coal and rock strata are shown in Table 6.

Lithology name	Bulk modulus	Shear modulus	Cohesion MPa	Internal friction angle°	Tension MPa	Density kg/m <sup>3</sup>
	GPa					
sandstone	3.46	1.65	2.02	33	2.12	2640
mesquite	9.36	3.90	7.21	34	3.11	2550
mudstone	7.50	3.01	5.60	47	4.35	2620
limestone	2.77	1.18	1.81	45	2.14	2580
coal	1.85	0.82	2.42	24	0.80	1400
siltstone	7.36	2.88	5.53	46	3.03	2530
sandy mudstone	2.73	1.50	2.40	43	1.90	2590
siltstone	3.46	1.65	2.02	33	2.12	2640

**Table 6.** Physical and mechanical parameters of coal seams.

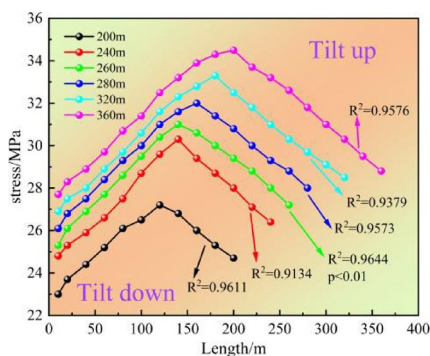


**Fig. 3.** Plot of the working face length versus roof stress.

Mining disturbances disrupt the original stress equilibrium in the complex coal seam structure, causing dynamic stress redistribution in the rock mass. As working face length changes, the stress orientation also shifts. After determining the optimal length through fuzzy comprehensive evaluation, computational modeling analyzed stress orientation distribution at different lengths. The results appear in Fig. 3.

The roof stress magnitude exhibits a strong length-dependent relationship. As working face length increases from 200 to 360 m, the maximum roof stress rises from 27.2 MPa to 34.5 MPa, a 26.8% increase. Vertical stress distribution analysis reveals a decaying increment rate with increasing length. As shown in Fig. 3, the stress growth rate reaches 9.9% at 260 m, when length increases further to 320 m, the maximum stress only rises 7.4%, from 31 MPa to 33.3 MPa. The inclined stress distribution shows higher stress levels in the upper and middle areas compared to the sides. This pattern results from geological factors including the increased inclination angle. The rock layer is prone to gravitational slip along the slope, which leads to the redistribution of stress in the upper and middle roof areas. Longer working face lengths alter load transfer mechanisms. Overlying rock layer loads travel longer paths to side coal pillars, increasing central region loading. Meanwhile, side coal pillars provide reduced support capacity. These combined effects create pronounced central stress concentration.

Roof plastic failure is a key indicator of rock mass instability in coal mining, directly threatening face safety and productivity. This occurs when mining-induced stress exceeds the rock mass strength, causing shear slip or tensile fracture propagation. As shown in Fig. 4, the plastic failure zone is primarily characterized by shear failure and expands with increasing working face length.

Within the 200–260 m range, the plastic zone grows gradually while maintaining a stable failure height. This stability arises because the key layer forms an effective rock beam structure, and collapsed goaf rock forms a supporting arch that shares the overlying strata load. When the face length exceeds 280 m, the key layer transitions from a beam to a slab structure, stress distribution becomes nonlinear, and the original support system becomes inadequate. This leads to notable intensification of plastic deformation, with failure height increasing from 10 m at 260 m to 18 m at 360 m. From the above analysis, it can be seen that the minimal change in plastic zone extent between 200 and 260 m contributes to maintained roof stability and enhanced working face safety.

Optimal working face length selection requires balanced consideration of multiple factors. These include mine design capacity requirements, roof stress minimization benefits, extended equipment service life under reduced stress, and lower maintenance costs. After analyzing the data fitting, the 260 m model demonstrates superior fitting performance with  $R^2 = 0.9644$  compared to 0.9573 for the 280 m case. The 260 m working face length provides higher polynomial fit significance, confirming model reliability. This value indicates how closely the model's simulated roof stress values (Y-axis) match the optimal regression curve across different working

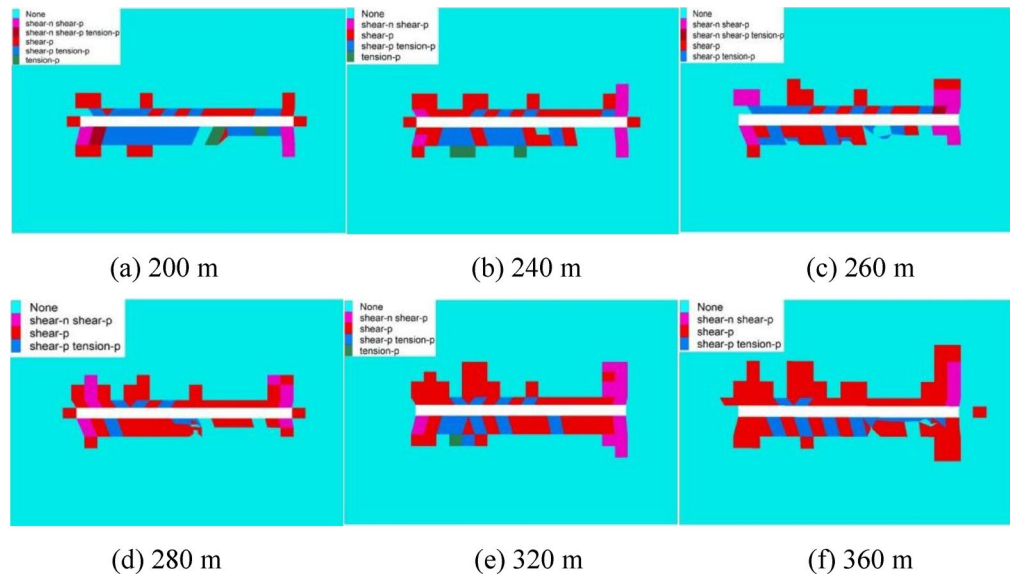


**Fig. 4.** Plasticized damage cloud diagram of the working face roof plate.

face lengths (X-axis). The above results confirm 260 m is optimal due to the effects of stress and economic costs in steeply dipping seams.

### Field application analysis

The 4103 working face is in the fourth mining area at 750 m in the eastern area. The coal seam has an inclination angle of 36.6–39.1° (average 37.7°) and thickness of 3.2–4.9 m (average 4.0 m, including gangue). The seam has a hardness of 1.86 and density of 1.39 t/m<sup>3</sup>. The face design includes recoverable reserves of 947,649 tons (actual recoverable 881,314 tons), with 5 daily production cycles over 28 operational days per month.

The production  $A$  and face length  $L$  maintain the functional relationship:

$$A = L \cdot v \cdot c \cdot H \cdot \gamma \quad (20)$$

Calculated:

$$L_{\min} = 253.59 \text{ m.}$$

Formula:  $A$ —Output of working face, taking 5245 t/d;  $L$ —working face length, m;  $V$ —Advancing speed of working face, taking 4 m/d;  $H$ —Coal seam thickness, taken as 4 m;  $\gamma$ —Unit weight of coal, 1.39 t/m<sup>3</sup>;  $C$ —Recovery rate of working face, taken as 0.93.

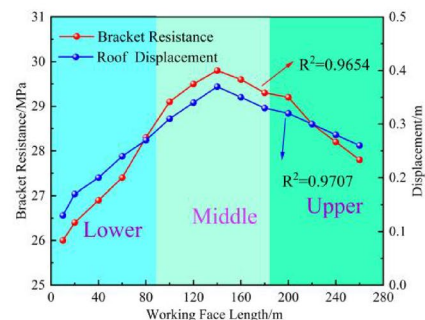
According to the formula of daily production combined with the fuzzy evaluation results, the working face length can be considered as 260 m.

Measuring points were established in the inclined area of the 4103 working face to assess roof rock pressure and subsidence variations under economically optimal length conditions. Three survey zones are established along the working face dip direction: the upper zone near the return airway (1<sup>#</sup>–55<sup>#</sup>), the middle zone (56<sup>#</sup>–121<sup>#</sup>), and the lower zone adjacent to the haulage roadway (122<sup>#</sup>–178<sup>#</sup>). Selected survey points include 5<sup>#</sup>, 15<sup>#</sup>, 35<sup>#</sup>, and 45<sup>#</sup> in the upper zone; 60<sup>#</sup>, 85<sup>#</sup>, 99<sup>#</sup>, and 115<sup>#</sup> in the middle zone; and 125<sup>#</sup>, 140<sup>#</sup>, 156<sup>#</sup>, and 170<sup>#</sup> in the lower zone. The resulting stress and displacement data appear in Fig. 5.

The 260 m working face showed characteristic support resistance distribution. Maximum resistance reached 29.8 MPa, a 2.5 MPa increase over shorter adjacent faces but still below the 35 MPa hydraulic support safety threshold. On-site monitoring curves confirmed significant consistency between hydraulic support resistance and displacement, revealing roof stress distribution patterns. Stress distribution remained relatively balanced in the middle and upper sections, reducing support maintenance frequency and extending service life. Roof subsidence monitoring indicated all values within reasonable ranges: central overburden showed maximum dynamic movement with 0.37 m subsidence, upper sections experienced secondary subsidence from gravitational slip, and lower sections displayed minimal movement due to dense gangue filling. These results quantitatively confirm that the 260 m optimized face length controls peak abutment pressure while maintaining roof subsidence below the 0.4 m safety threshold, ultimately improving production efficiency.

Monitoring data demonstrate that at 260 m face length, both hydraulic support working resistance and roof subsidence remain within low ranges, reducing roof accident risks while ensuring safe and efficient production.

To validate the working face configuration, costs were compared with the adjacent 1508 face (240 m length, 1.67 Mt output). The 1508 face recorded a total cost of 130.2 yuan/t, including 30.54 million yuan for tunneling, 16.5 million for labor, 8.2 million for relocation, 113.85 million for maintenance, and 48.3 million for transportation. The operational 4103 face (260 m length) has produced 0.36 Mt with a lower cost of 128.6 yuan/t, consisting of 16.04 million for tunneling, 3.15 million for labor, 9 million for relocation, 11.25 million for



(a) Working Face Field Conditions Diagram

(b) Support Resistance and Displacement Distribution at 260 m Face

Fig. 5. 4103 working face analysis diagram.

maintenance, and 6.84 million for transportation. Initial results confirm the economic advantage of the 260 m face. Subsequent analysis will incorporate late-stage maintenance costs for comprehensive validation.

## Conclusion and future work

- (1) The fuzzy comprehensive evaluation method effectively quantified weight coefficients for cost parameters through multi-factor assessment. The resulting composite score identified 260 m as the economically optimal working face length, balancing operational requirements with economic considerations.
- (2) Numerical simulations confirmed that 260 m represents the critical threshold for roof stability in steeply dipping seams (35°–55°). At this length, roof stress maintained at 31 MPa with controlled plastic zone development (8–10 m height), while exceeding 280 m triggered nonlinear stress increases to 34.5 MPa and plastic zone expansion to 15–18 m.
- (3) Field monitoring at the 4103 working face demonstrated that the 260 m configuration maintained support resistance below 29.8 MPa and roof subsidence under 0.37 m, both within safety thresholds. The balanced stress distribution reduced maintenance frequency compared to longer face configurations.
- (4) Current model parameters apply to specific geological conditions and lack validation under broader geological settings. Economic parameters reflect current market conditions and may be affected by energy price and labor cost fluctuations. Future studies will develop models using real-time monitoring and machine learning to dynamically optimize working face parameters across varying geological and economic conditions, improving model generalizability and practical utility.

## Data availability

The datasets generated during and/or analysed during the current study are available from the corresponding author on reasonable request.

Received: 24 July 2025; Accepted: 27 October 2025

Published online: 26 November 2025

## References

1. Chen, D., Sun, C. & Wang, L. Collapse behavior and control of hard roofs in steeply dipping coal seams. *Bull. Eng. Geol. Env.* **80**(2), 1489–1505. <https://doi.org/10.1007/s10064-020-02014-3> (2021).
2. Yan, Y., Zhang, Y., Zhu, Y., Cai, J. & Wang, J. Quantitative study on the law of surface subsidence zoning in steeply dipping extra-thick coal seam mining. *Sustainability* **14**(11), 6758. <https://doi.org/10.3390/su14116758> (2022).
3. Zhen, E. et al. Analysis of the EFARC non-pillar mining stope: roof failure and overlying pressure in inclined coal seams. *Geomech. Geophys. GeoEnergy GeoResour.* **9**(1), 151. <https://doi.org/10.1007/s40948-023-00691-4> (2023).
4. Jia, C. et al. Study on multisize effect of mining influence of advance speed in steeply dipping extrathick coal seam. *Lithosphere* **2022**(Special10), 9775460 (2022).
5. Wu, F. et al. Study on failure characteristics and reasonable mining parameters of upward mining of integrated coal mine. *Geofluids* **2022**(1), 4647558. <https://doi.org/10.1155/2022/4647558> (2022).
6. Wang, C. X. et al. Establishment of the roof model and optimization of the working face length in top coal caving mining. *Geomech. Eng.* **36**(5), 427–440. <https://doi.org/10.12989/gae.2024.36.5.427> (2024).
7. Ordín, A. A. & Metelkov, A. A. Optimization of the fully-mechanized stoping working face length and efficiency in a coal mine. *J. Min. Sci.* **49**(2), 254–265. <https://doi.org/10.1134/s106273914902007x> (2013).
8. Zhao, G., Zhang, B., Zhang, L., Liu, C. & Wang, S. Roof fracture characteristics and strata behavior law of super large mining working faces. *Geofluids* **2021**(1), 8530009. <https://doi.org/10.1155/2021/8530009> (2021).
9. Xue, B., Wang, C., Wang, Y., Zhang, W. & Yang, S. An investigation of the coal wall zoning failure patterns resulting from the changes in support parameters of large mining height. *Mech. Time Depend. Mater.* **28**(4), 2599–2618. <https://doi.org/10.1007/s11043-023-09660-6> (2024).
10. Zhang, J. et al. Roof stability analysis model of super-long fully mechanized working face and its application. *Geomech. Geophys. GeoEnergy GeoResour.* **10**(1), 1–13. <https://doi.org/10.1007/s40948-024-00908-0> (2024).

11. Ding, Z. et al. Reasonable working-face size based on full mining of overburden failure. *Sustainability* **15**(4), 3351. <https://doi.org/10.3390/su15043351> (2023).
12. Wang, H. et al. Three-peak evolution characteristics of supporting stress on a super-long working face in a thick coal seam. *Front. Energy Res.* **11**, 1238246. <https://doi.org/10.3389/fenrg.2023.1238246> (2023).
13. Meng, G. H. et al. Bearing characteristics and safety control of hydraulic support groups in shallow-buried thin bedrock ultra-long working faces. *J. Central South Univ.* **30**(5), 1662–1674. <https://doi.org/10.1007/s11771-023-5313-9> (2023).
14. Huang, P. et al. Multiscale study on coal pillar strength and rational size under variable width working face. *Front. Environ. Sci.* **12**, 1338642. <https://doi.org/10.3389/fenvs.2024.1338642> (2024).
15. Wang, X. et al. Model test study on overburden failure and fracture evolution characteristics of deep stope with variable length. *Adv. Civil Eng.* **2022**(1), 9818481. <https://doi.org/10.1155/2022/9818481> (2022).
16. Tong, X. et al. Transient electromagnetic perspective technology in the ultra-long coal mining face. *J. Appl. Geophys.* **223**, 105353. <https://doi.org/10.1016/j.jappgeo.2024.105353> (2024).
17. Liu, X. et al. Surface damage reduction effect of ultra-high working face in Shangwan coal mine. *Sci. Rep.* **14**(1), 21196. <https://doi.org/10.1038/s41598-024-72261-x> (2024).
18. Liu, B., & Zhang, Q. (2019, December). Reason analysis and prevention measures of abnormal O<sub>2</sub> concentration in return air corner of super-long mining working face of shallow depth seam. In *IOP Conference Series: Earth and Environmental Science* (Vol. **358**, No. **3**, p. **032030**). IOP Publishing. <https://doi.org/10.1088/1755-1315/358/3/032030>
19. Li, J. & Ding, R. Research on comprehensive evaluation indicators and methods of world-class open-pit coal mines. *Sustainability* **16**(18), 8134. <https://doi.org/10.3390/su16188134> (2024).
20. Song, D. et al. Feasibility evaluation of highwall mining in open-pit coal mine based on method of integrated analytic hierarchy process-fuzzy comprehensive evaluation-variable weight theory. *Electronics* **12**(21), 4460. <https://doi.org/10.3390/electronics12214460> (2023).
21. Liu, X., Liu, H., Wan, Z., Pei, H. & Fan, H. The comprehensive evaluation of coordinated coal-water development based on analytic hierarchy process fuzzy. *Earth Sci. Inf.* **14**, 311–320. <https://doi.org/10.1007/s12145-020-00523-z> (2021).
22. Zhu, Z., Wu, Y. & Han, J. A prediction method of coal burst based on analytic hierarchy process and fuzzy comprehensive evaluation. *Front. Earth Sci.* **9**, 834958. <https://doi.org/10.3389/feart.2021.834958> (2022).
23. Du, X., Fang, H., Liu, K., Xue, B. & Cai, X. Environmental evaluation of coal mines based on generalized linear model and nonlinear fuzzy analytic hierarchy. *Geofluids* **2020**(1), 8836908. <https://doi.org/10.1155/2020/8836908> (2020).
24. Meng, Q., Wu, Y., Zhang, M., Wang, Z. & Lei, K. Stability assessment of deep three-soft outburst coal seam roof based on fuzzy analytic hierarchy process. *Shock. Vib.* **2021**(1), 4328550. <https://doi.org/10.1155/2021/4328550> (2021).
25. Janthasuwan, U., Niwitpong, S. & Niwitpong, S. A. Confidence intervals for coefficient of variation of Delta-Birnbaum-Saunders distribution with application to wind speed data. *AIMS Math.* **9**(12), 34248–34269. <https://doi.org/10.3934/math.20241631> (2024).
26. Zhang, B. et al. A groundwater quality assessment model for water quality index: Combining principal component analysis, entropy weight method, and coefficient of variation method for dimensionality reduction and weight optimization, and its application. *Water Environ. Res.* **96**(12), e11155. <https://doi.org/10.1002/wer.11155> (2024).
27. Zhang, R. et al. Risk assessment of compound dynamic disaster based on AHP-EWM. *Appl. Sci.* **13**(18), 10137. <https://doi.org/10.3390/app131810137> (2023).
28. Li, S. et al. Analysis of coal mine environment corrosion tendency based on fuzzy comprehensive evaluation method. *Coal Sci. Technol.* **53**(5), 52–63. <https://doi.org/10.12438/cst.2024-0150> (2025).
29. Zadeh, L. A. A rationale for fuzzy control. *Fuzzy Sets Fuzzy Logic Fuzzy Syst. Sel. Papers Lotfi A Zadeh* [https://doi.org/10.1142/9789814261302\\_0009](https://doi.org/10.1142/9789814261302_0009) (1996).
30. Wu, H. C. *Mathematical foundations of fuzzy sets* (John Wiley & Sons, 2023).

## Author contributions

Z. G. was involved in the conception and design, revising it critically for intellectual content, and the final approval of the version to be published. H. Z. was involved in the conception and design, the drafting of the paper, and the final approval of the version to be published. I. M. and Y. L. analysis and interpretation of the data, and the final approval of the version to be published.

## Declarations

## Competing interests

The authors declare no competing interests.

## Additional information

**Correspondence** and requests for materials should be addressed to Z.G.

**Reprints and permissions information** is available at [www.nature.com/reprints](http://www.nature.com/reprints).

**Publisher's note** Springer Nature remains neutral with regard to jurisdictional claims in published maps and institutional affiliations.

**Open Access** This article is licensed under a Creative Commons Attribution-NonCommercial-NoDerivatives 4.0 International License, which permits any non-commercial use, sharing, distribution and reproduction in any medium or format, as long as you give appropriate credit to the original author(s) and the source, provide a link to the Creative Commons licence, and indicate if you modified the licensed material. You do not have permission under this licence to share adapted material derived from this article or parts of it. The images or other third party material in this article are included in the article's Creative Commons licence, unless indicated otherwise in a credit line to the material. If material is not included in the article's Creative Commons licence and your intended use is not permitted by statutory regulation or exceeds the permitted use, you will need to obtain permission directly from the copyright holder. To view a copy of this licence, visit <http://creativecommons.org/licenses/by-nc-nd/4.0/>.

© The Author(s) 2025